

# VISUALISATION OF VORTEX-FLAME INTERACTIONS IN A COUNTERFLOW DIFFUSION FLAME

Illari Vihinen, James R. Gord, Jeffrey M. Donbar, Gregory J. Fiechtner,  
Campbell D. Carter, and J. C. Rolon

**Keywords:** *Extinction, laminar flames, vortex, digital PIV, turbulence*

## Abstract

*The dynamic interaction between a laminar flame and a vortex is examined. The hydroxyl (OH) layer produced by the flame is imaged using planar laser-induced fluorescence (PLIF), and preliminary vortex-characterisation data are acquired using acetone PLIF and digital, two-colour particle-image velocimetry (PIV). The hydrogen-air flame is supported in a nonpremixed opposed-jet burner. The apparatus is found to produce highly repeatable events, making it ideal for studying the interaction between a flame and an isolated vortex. A distinct annular extinction of the OH layer is observed, in good agreement with previous computational modeling predictions of the apparatus. In cases with no extinction of the OH layer, enhanced burning is observed during the vortex-flame interaction.*

## 1 Introduction

Recent results in numerical modelling combined with experimental measurements have led to important advances in the understanding of combustion. Numerous investigations have

contributed to these advances, including a particular type of study in which the interaction between a laminar, nonpremixed flame and a vortex is examined. These experiments involve repeatable, carefully controlled conditions that are highly amenable to experimental study.

In recent computational calculations, Katta [1] predicted that, during the interaction of a nonpremixed hydrogen-air flame and an isolated vortex, the extinction of the OH layer would occur in an annular pattern. The experiments detailed in this paper are carried out to examine, in part, the validity of this prediction. Experimental results obtained with planar laser-induced fluorescence (PLIF) of OH are used to determine regimes in which the annular, Katta-type extinction occurs. The nonpremixed flame is supported by air and fuel in an opposed-jet burner. The fuel consists of hydrogen diluted with nitrogen. The amount of hydrogen in nitrogen is varied, along with the strength of the vortex. The temporal evolution of vortex-flame interactions is imaged with the PLIF system.

Recently, additional measurements have been initiated for characterisation of vortices. First, acetone is seeded into the vortex and its laser-excited fluorescence is detected. Second, particles are seeded into the flowfield, and the scattering is used for digital, two-colour particle-image velocimetry (PIV) measurements. Preliminary results from the use of both techniques are discussed in this paper.

## 2 Background

Numerous experimental studies of the interaction dynamics of vortices and flames have been conducted, and many of these investigations employed two-dimensional imaging to study the

**Author(s):** *Illari Vihinen,<sup>1</sup> James R. Gord,<sup>1</sup> Jeffrey M. Donbar,<sup>1</sup> Gregory J. Fiechtner,<sup>2</sup> Campbell D. Carter,<sup>2</sup> J. C. Rolon<sup>3</sup>*

<sup>1</sup>*Propulsion Directorate, Air Force Research Laboratory, Wright-Patterson Air Force Base, OH 45433-7103, USA.*

<sup>2</sup>*Innovative Scientific Solutions, Inc., 2786 Indian Ripple Road, Dayton, OH 45440-3638, USA.*

<sup>3</sup>*Laboratoire d'Énergétique Moléculaire et Macroscopique, Combustion, École Centrale Paris, Grande Voie des Vignes, 92295 Châtenay-Malabry Cedex, France.*

interaction. For premixed flame fronts, most measurements have been made using two types of flames. Hertzberg et al. [2] and Escudie [3] conducted an experiment in which a Karman vortex street was produced using a cylindrical rod in a cross flow of premixed gases. A V-flame was supported behind a wire positioned downstream of the rod that produced the vortex street. Planar tomographic imaging was used to study the interaction of the vortex street with the flame. A similar interaction between a Karman vortex street and a flame was investigated by Lee et al. [4] using PLIF imaging of OH and by Nye et al. [5] using both OH PLIF and PIV. A disadvantage of the vortex street is the difficulty in isolating a single vortex. Nguyen and Paul [6] studied a more isolated interaction by replacing the Karman vortex street with a vortex directed into one side of a V-flame. The vortex-injection process was found to be highly repeatable.

In a second type of study involving premixed combustion, Jarosinski et al. [7] studied a flame that was ignited at one end of a tube of premixed gases. A vortex was injected at the other end of the tube. The interaction dynamics were then photographed using a mercury-xenon arc lamp and a rotating-drum streak camera with a rotating-disc shutter. Recently, Driscoll and co-workers produced an impressive series of papers concerning a similar vortex-flame apparatus in which either PIV or OH PLIF (or a combination of these imaging techniques) was applied [8-18].

Nonpremixed flames have also been the subject of experimental investigation. Rolon and co-workers [19, 20] recently developed an apparatus in which a vortex is injected into a flame supported between the nozzles of an opposed-jet burner. This geometry has numerous advantages. First, a stationary flame can easily be produced and isolated. Second, the flame thickness can be varied by changing either the nozzle velocities or the spacing between the upper and lower burner nozzles. More recently, Chen and Dahm [21] developed a facility for generating a nonpremixed burning layer that wraps into a vortex ring. The resulting combustion is studied under conditions of normal gravity and microgravity.

The experiments described in this paper are based on the counterflow geometry of Rolon and

co-workers, and the observations described below rely heavily on the progress outlined in their papers [19, 20]. A fuel mixture of hydrogen and nitrogen allows the use of laser diagnostics in the absence of hydrocarbon interferences, and the reaction zone of these nonpremixed flames is generally much thicker than that for premixed flames. The comparatively simple hydrogen-chemistry mechanisms simplify numerical calculations that are the subject of comparison with experimental results.

### 3 Apparatus and Procedure

#### 3.1 Burner Facility

A picture (a) and diagram (b) of the burner are shown in Figure 1. The configuration is based on the design of Rolon et al. [19, 20]. The flame is supported between upper and lower nozzles separated by 40 mm, each with an exit diameter of 25 mm. The fuel consists of hydrogen diluted with nitrogen and flows from the upper nozzle. Air flows from the lower nozzle. Unique to this type of apparatus is a tube with 5-mm inner diameter that is installed concentrically within the lower nozzle. This tube is attached to a cylinder that contains a piston, which in turn is attached to an actuator. Feeding an appropriate current to the actuator causes a solenoid to force the piston upward abruptly, resulting in the emergence of a vortex from the tube. The vortex travels upward within the surrounding oxidizer flow. A flow of air is supplied to the vortex tube such that in the absence of a vortex, the exit velocity matches the velocity of the air from the surrounding nozzle. To minimize the impact of room-air disturbances, upper and lower guard flows of nitrogen are supported through outer nozzles, which are concentric with the respective upper and lower inner nozzles that support the flame.

The hydrogen, nitrogen diluent, and oxidizer air flows are furnished by mass-flow controllers with full-scale ranges of 20 l/m, 20 l/m, and 30 l/m, respectively. A continuous flow of air is provided to the vortex tube by a 5-l/m controller, while the guard flow from the upper and lower guard (outer) nozzles is furnished by two 50-l/m

mass flow controllers. The flow rates of each controller are good to  $\pm 1\%$  of the full-scale range. The experiments have been repeated for several different flame conditions, as summarized in Table I.

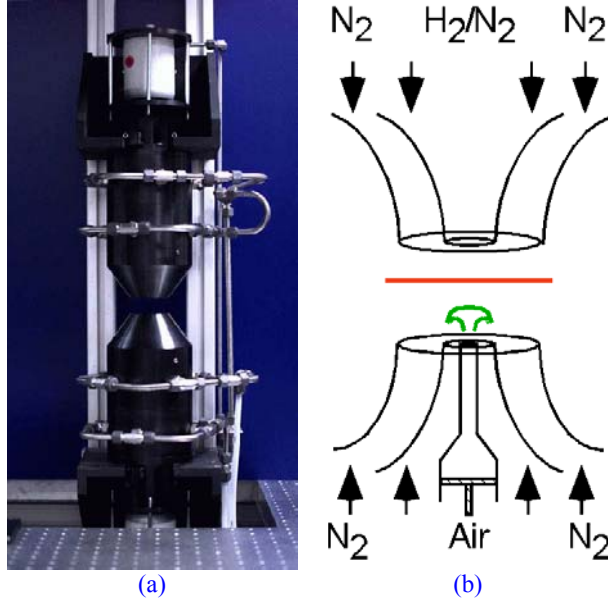


Figure 1: (a) Digital photograph of the opposed-jet burner. (b) Cross-sectional diagram of the burner nozzles and piston; the flame is red, the air vortex is green.

Table I: Flow rates (l/m) at 21.5°C and 724 mm Hg for five flame conditions.  $X_{H_2}$  is the volume fraction of hydrogen in nitrogen diluent.

Gas	Flame					
	A	B	C	D	E	F
H <sub>2</sub>	2.76	3.40	4.04	4.67	5.31	5.94
N <sub>2</sub> Diluent	17.1	17.1	17.1	17.0	17.0	16.9
$X_{H_2}$	0.14	0.17	0.19	0.22	0.24	0.26
Air	11.2	11.2	11.2	11.2	11.2	11.2

The vortex properties can be varied by changing the magnitude and the rise time of the current that is fed to the actuator. The impedance of the actuator ranges from 1  $\Omega$  to 1.5  $\Omega$ , depending on the frequency content of the current. At full displacement, a current of up to 6 A is provided to the solenoid by a specially designed, high-speed power amplifier. This can result in considerable power consumption by the actuator if the full displacement condition is maintained

for long periods of time. Consequently, an AC waveform is supplied by the initial application of a negative potential, causing the piston to be withdrawn away from the flame. The negative potential is applied for about 0.5 s to allow the flame to recover from this initial disturbance, which is verified by digital, two-colour PIV. The potential is then quickly changed to a positive value of the same magnitude with a carefully controlled rise time,  $\tau_r$ . The strength of the vortex can be increased by increasing the current magnitude, which results in a larger displaced fluid volume through the exit of the tube. Eventually, the maximum displacement of the solenoid is reached. In this case, the vortex strength can also be increased using a smaller value of  $\tau_r$ . The relationship among volume displacement,  $\tau_r$ , and the vortex characteristics has been discussed in numerous papers, including those by Rolon et al. [19], Roberts [9], and Chen and Dahm [21]. The drive current for the solenoid is obtained by power amplifying the output of a digital arbitrary-waveform generator. This generator is operated at its maximum number of 10,000 quantized steps, resulting in a minimum stepsize of 0.1 ms. For all measurements discussed in this paper,  $\tau_r$  is set at 10 ms.

Visualisation of the vortex formation and propagation via acetone PLIF is accomplished using a vaporiser that is installed between the vortex tube and the mass-flow controller. A bypass valve allows the choice of acetone seeding level. Because the acetone changes the flame characteristics, these visualisation studies are limited to non-reacting flows. When the acetone studies are not required, the acetone vaporiser is removed from the apparatus.

Seed particles are introduced into the burner flows when digital PIV measurements of the velocity of the vortex are performed. Three particle seeders are installed: One seeder is placed after the oxidiser-air mass-flow controller and another after the vortex-air mass-flow controller. The third seeder is installed after the junction where the hydrogen and nitrogen gases are mixed. With the use of three seeders, each flow can be seeded with particles individually, or combinations of the different flowfields can be

seeded. Each seeder contains hollow spherical ceramic particles with an approximate mean diameter of 2.4  $\mu\text{m}$ . When PIV studies are not required, the seeders are removed from the apparatus.

### 3.2 Laser Diagnostics

The PLIF system contains a frequency doubled, Q-switched Nd:YAG laser that is used to pump a dye laser which is, in turn, frequency doubled. The light is directed through a telescope that is adjusted to produce a light sheet with a height that matches as nearly as possible the 40-mm burner separation. The resulting beam thickness is  $\sim 300 \mu\text{m}$ , which corresponds to the full width at 25% of the peak of the intensity profile, and  $\sim 15 \text{ mJ/pulse}$  is available at the test section.

Hydroxyl radicals absorb the laser radiation at 281.3414 nm via the  $R_1(8)$  transition of the (1,0) band in the A-X system. Fluorescence from the A-X (1,1) and (0,0) bands is detected at right angles through WG-295 and UG-11 coloured-glass filters, followed by a 105-mm focal length, f/4.5 UV lens. The resulting light reaches an intensified CCD camera with an intensifier gate width of 100 ns. CCD pixels are binned in groups of 2x2. Data are stored on a personal computer. A colour table is used with a maximum value set to 95% of the maximum signal for all images taken at a given flame condition. The low-signal colour is assigned by calculating the background noise and selecting a minimum value that is two standard deviations above this level. Therefore, in cases where “extinction” of the OH layer is observed, “extinction” refers to signal levels that fall below this minimum value and are, therefore, assigned the last colour in the table. All images represent the signal collected during a single laser shot, and no smoothing of the resulting images is attempted.

In studies of vortex-flame interactions by other investigators [22], LIF was applied as a marker of some other quantity such as heat release or burning rate. In the present experiments, the OH image is obtained for direct comparison with numerical computations of the OH distribution [1]; therefore, no attempt is made to correlate the images with any other quantities.

Acetone PLIF imaging is accomplished using the OH PLIF imaging system. Here, the UG-11 coloured-glass filter is removed to permit collection of the acetone fluorescence.

Recent measurements of the velocity field have been implemented using digital, two-colour PIV [23, 24]. Here, the ICCD camera is replaced with a colour digital CCD [25]. This type of CCD has a mask with green-transmissive filters for 50% of the pixels, red-transmissive filters for 25% of the pixels, and blue-transmissive filters for the remaining 25% of the pixels. Two lasers are used, with one sheet being produced by directly doubling the output of a Q-switched Nd:YAG laser (30 mJ/pulse at the test section). The second light sheet is produced by pumping a dye laser (employing DCM laser dye) with a second frequency-doubled, Q-switched Nd:YAG laser, resulting in laser radiation at 640 nm (40 mJ/pulse at the test section). The thickness of both the red and green sheets is set to  $\sim 700 \mu\text{m}$ . A digital delay generator is used to drive the timing of the two lasers such that the red pulses are delayed by a precisely controlled amount of time with respect to the green pulses. In the absence of a vortex, the underlying counterflow velocity field is probed with red pulses that are delayed by up to 1 ms with respect to the corresponding green pulses. For the fastest vortices studied, the delay between red and green pulses is reduced to 10  $\mu\text{s}$ . The camera shutter is set to be open for 1/15 s to permit both laser pulses to be detected by the colour CCD. Most of the flame emission and light emitted by other devices in the laboratory (monitors, etc.) is greatly attenuated by the shutter. Velocity vectors are calculated using the correlation software of Gogenini and co-workers [23].

### 3.3 Synchronisation and Timing

Precise synchronisation of several experimental events, including vortex generation and propagation, production of laser pulses, and activation of the camera shutter or intensifier, is required. A block diagram of the synchronisation scheme is shown in Figure 2.

Because the Nd:YAG lasers are designed to operate at a nominal repetition rate of 10 Hz, the experimental sequence must be synchronised to a

10-Hz master clock that drives the flash lamps the AWG waveform is initiated, the vortex is

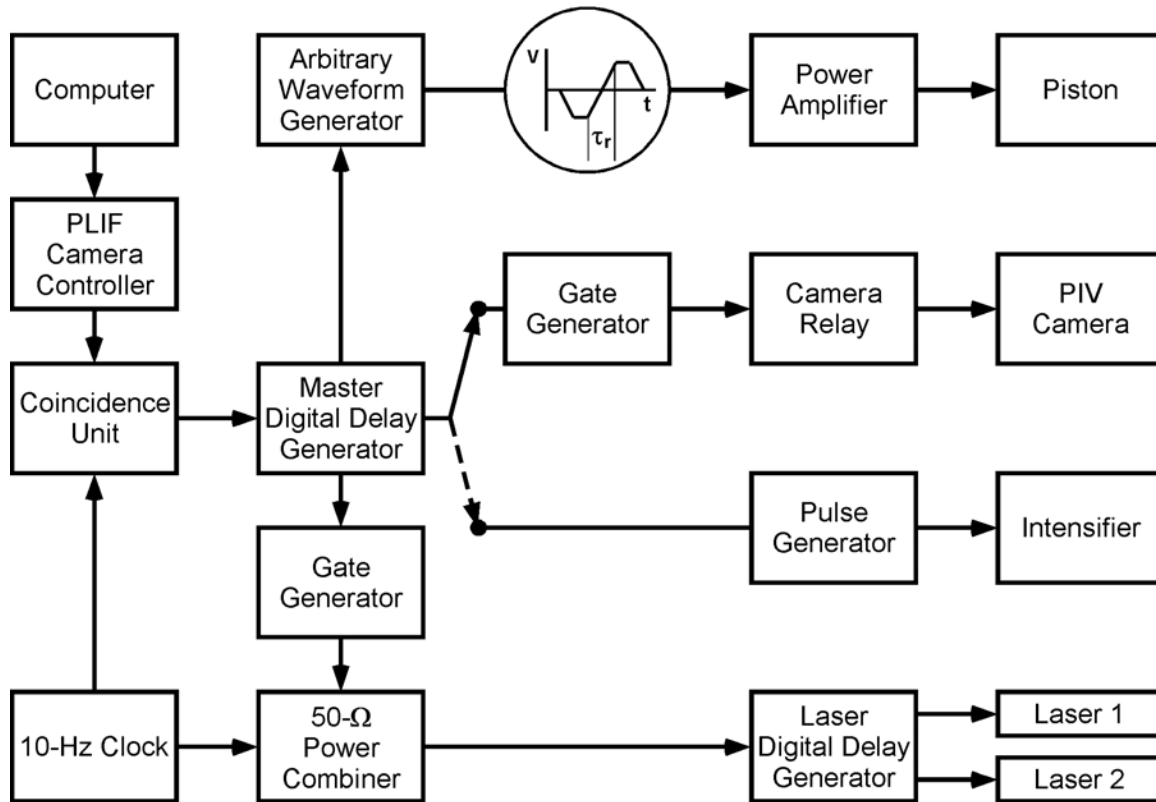


Figure 2: Diagram of electronic timing connections.

and the Pockels cells of the lasers. To trigger the laser(s), the clock sends two signals, one of which travels to a 50-Ω power combiner and then the laser digital delay generator (DDG). The 10-Hz clock also provides a TTL signal to one of two inputs of a coincidence unit. The second input of the coincidence unit is driven by a TTL pulse from the PLIF camera controller. The coincidence unit outputs a pulse only when pulses from both the 10-Hz clock and the PLIF camera controller are present. When a vortex-flame event is initiated using a personal computer, the PLIF camera controller outputs a pulse approximately 1.3 s in duration. The corresponding output of the coincidence unit is a 1.3-s envelope of TTL pulses spaced by 100 ms. The first pulse in this envelope triggers a master DDG, synchronising it with the 10-Hz clock and the laser pulse train. This DDG triggers an arbitrary-waveform generator (AWG) that outputs a 1-s waveform, which is amplified and fed to the piston actuator to generate a vortex. Approximately 0.5 s after

fired; therefore, five laser pulses are generated during the time between computer initiation and the vortex-flame interaction.

When the DDG is externally triggered, the jitter between the trigger and a DDG output pulse is 60 ps plus the output delay divided by  $10^8$ . Over the 0.5-s period between the first and fifth laser pulses, this corresponds to a jitter of 5.06 ns. The DDG clock jitter specifications are not nearly so good. The jitter between clock outputs is 1 part in 10,000, corresponding to a jitter of 50 μs over the same 0.5-s period. Attempting to synchronise the piston with the clock severely limits the temporal resolution available to “freeze” vortex-flame events in time and requires an intensifier gate width significantly larger than 50 μs. The master DDG is therefore configured to trigger preemptively the fifth laser pulse. A delayed pulse from the master DDG arrives at the 50-Ω power combiner just before the fifth pulse in the clock pulse train, preemptively triggering the laser(s). If no initiation pulse is output from

the computer, the laser(s) are triggered by the 10-Hz clock as usual. This approach reduces the jitter in the timing of the fifth laser pulse from 50  $\mu$ s to approximately 5 ns while maintaining the nominal 10-Hz repetition rate required by the lasers.

Another output of the master DDG is suitably delayed and directed to the image detector. For PIV experiments, the width of this TTL pulse is adjusted using a gate generator, which closes a relay to trigger the digital PIV camera system. For PLIF experiments, this master DDG output triggers a pulse generator, which, in turn, activates the intensifier of an ICCD camera.

The scheme depicted in Figure 2 provides precise control of the relative timing between the laser diagnostics and the vortex-flame event. To explore the temporal evolution of the event, data are captured utilising this phase-locked timing sequence: 1) an image is recorded, 2) the delay between vortex production and the laser/camera events is adjusted, and 3) another vortex is initiated and a second image is recorded. This process is repeated to acquire numerous images, each obtained at increasing delay, then an animation is created by assembling the individual images in temporal order. Effective temporal separation between images is selected between 10  $\mu$ s and 200  $\mu$ s, depending on the time scale of the event under study. The resulting animations are a testament to the high degree of repeatability achievable with this apparatus.

## 4 Results and Discussion

### 4.1 Vortex Characterisation

The sequence of acetone images in Figure 3 is typical of the sequential images used to measure the vortex propagation velocity for a given amplitude and rise time of the solenoid drive current. The six images in the figure are selections from a sequence of 50 images, each delayed by 100  $\mu$ s relative to the previous image. If the location of the flame front in the absence of a vortex is known, the acetone PLIF image sequence can be used to estimate the velocity of the vortex at this location. In this case, the propaga-

tion velocity is  $\sim 5$  m/s. The animation of Figure 4 contains the full series of 50 images.

Recently, characterisation of vortex properties has been initiated using PIV. For example, Figure 5 contains the scattering signal obtained when seeding the vortex-tube flow with a slightly higher particle density than that produced by the upper- and lower-burner seed levels. The corresponding set of vectors is shown in Figure 6. The maximum vector length in the forward direction yields a propagation velocity of 0.77 m/s. Digital, two-colour PIV measurements are readily made when the flame is burning, offering a significant advantage over the acetone PLIF measurements of the vortex propagation velocity.

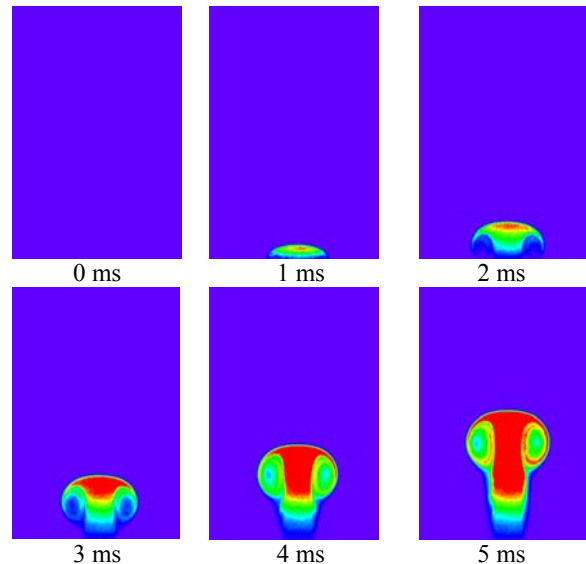


Figure 3: Acetone PLIF images of vortex.

### 4.2 Regimes of Vortex-Flame Interaction

The PLIF images of OH shown in Figure 7 correspond to a vortex-flame interaction in which extinction of the OH layer is absent. Initially, the vortex creates a small dent in the flame, and this dent then grows. Eventually the flame nearly surrounds the advancing vortex as it approaches the upper nozzle. In the later interaction stages, the OH PLIF signal level is observed to increase by up to a factor of five over the levels observed without a vortex. The increased signal level is indicated by the yellow colours in the frames of Figure 7. This change in OH signal level is thought to indicate enhanced burning. For this

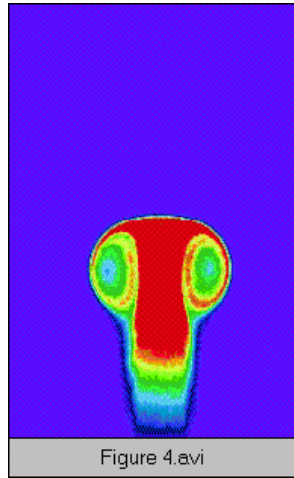


Figure 4: Animation of vortex motion.

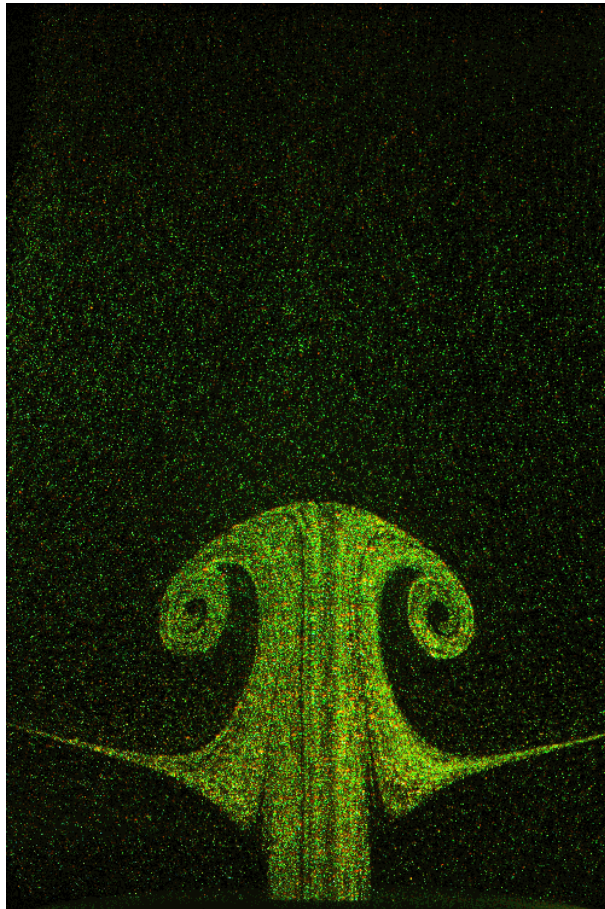


Figure 5: Scattering from particles in vortex flow.

particular example, the flow rates of Flame D of Table I are used. The animation of Figure 8

corresponds to an effective temporal delay of 200  $\mu\text{s}$  between each of the 92 frames.

The images of Figure 9 are obtained with flow conditions corresponding to Flame E of Table I. Extinction of the OH layer takes place in an annular pattern around the sides of the vortex, leaving a burning layer at its leading edge. This behaviour was first predicted numerically by Katta [1], well before these experiments were initiated, attesting to the utility of his code. After extinction, the isolated island of flame burns away, and the vortex travels upward toward the other nozzle. The flame follows the vortex, travelling up the stem. As the flame overtakes the vortex, it wraps up and turns in on itself. The entire sequence is illustrated in the animation of Figure 10, corresponding to a temporal delay of 200  $\mu\text{s}$  between each of the 73 frames.

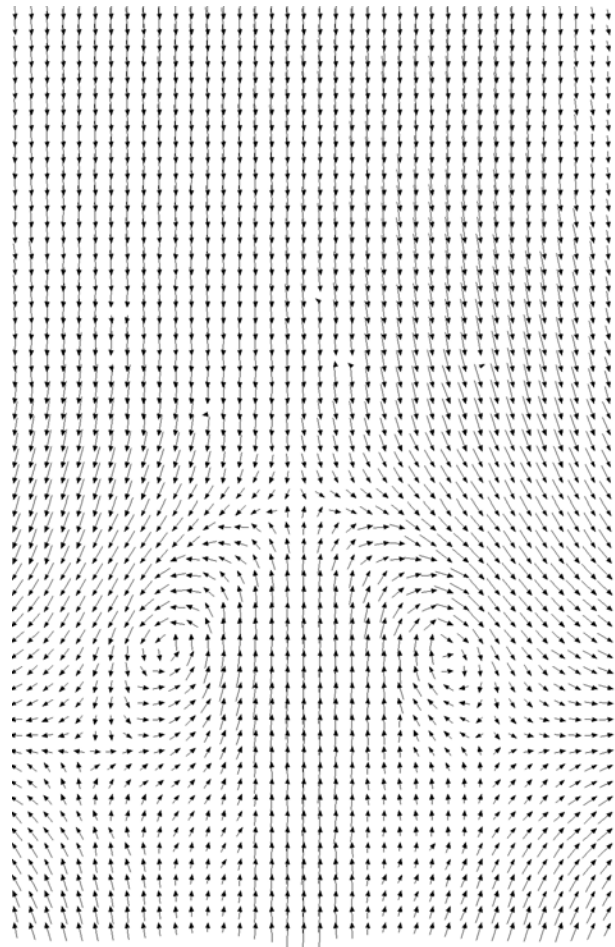


Figure 6: Vectors calculated from the PIV image of Figure 5.

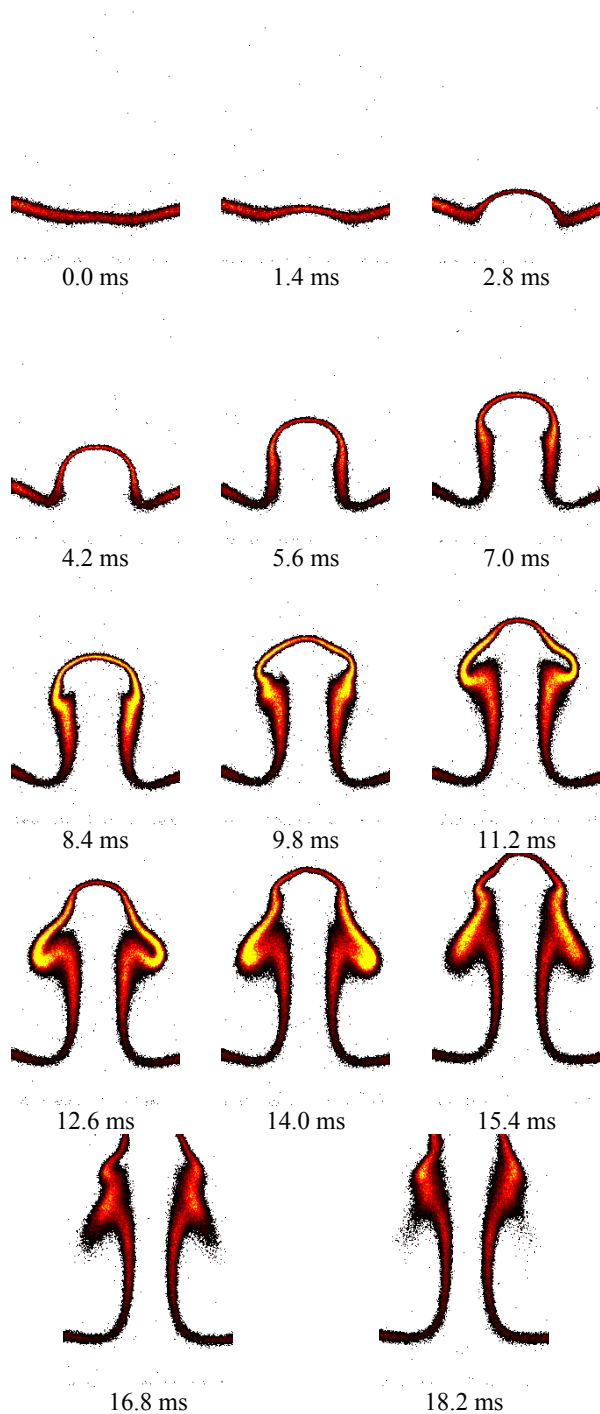


Fig. 7. OH PLIF images when OH layer remains intact.

The animation of Figure 11 was constructed to focus on the so-called Katta effect. Here, the temporal delay between frames is reduced to  $10 \mu\text{s}$ . The 50 frames in this animation were obtained in sequential order; images were not

reshuffled to make the animation smoother. As demonstrated in Figure 11, the repeatability of the apparatus of Rolon et al. [19, 20] is exceptional.

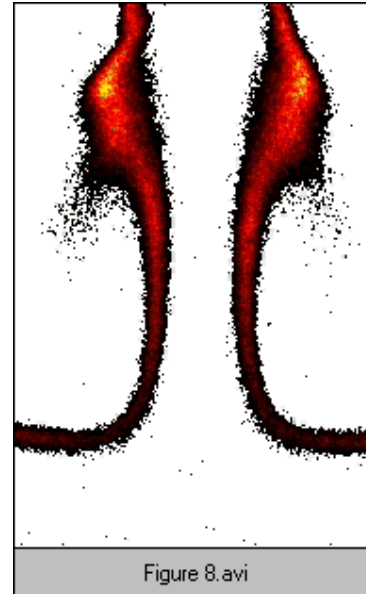


Figure 8: Animation corresponding to the images of Figure 7.

## 5 Conclusions and Future Research

The apparatus of Rolon and co-workers [19, 20] has been implemented for the study of the interaction of a flame with a vortex. PLIF measurements of acetone and digital, two-colour PIV have been applied to characterise the vortices injected into the opposed-jet flow. PLIF images of OH have been used to observe the dynamics of the interaction of the flame with the vortex. These combined measurements show that this burner can provide effective temporal resolution to at least the  $10\text{-}\mu\text{s}$  level. An annular break in the OH layer has been observed in excellent agreement with the numerical computations of Katta [1].

Future work will be directed toward the understanding of phenomena such as the Katta-type extinction. A variety of parameters can be studied, such as extended ranges of nitrogen dilution in hydrogen, different flame-thickness regimes, and different fuels. To aid in these studies, simultaneous OH PLIF and digital, two-colour PIV are presently being implemented,

along with measurements of the temperature field.

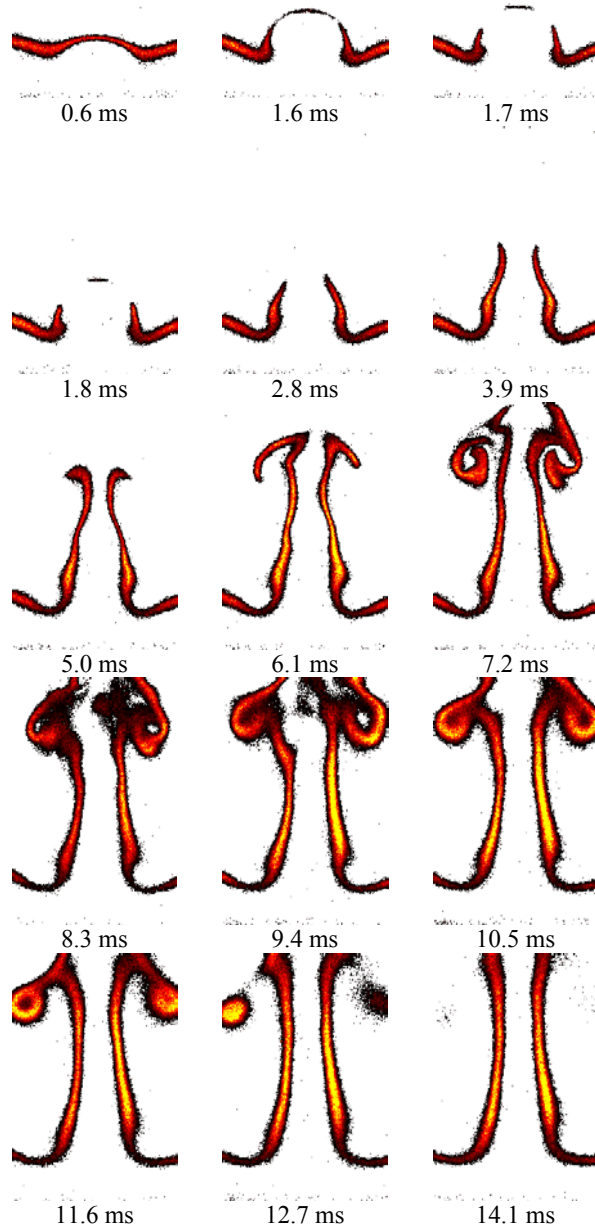


Figure 9: Sequence of images before and after extinction of the OH layer.

## 6 Acknowledgements

The authors are grateful to Mr. K. D. Grinstead, Jr., for assistance in synchronisation of the

experiment and construction of the solenoid-current power amplifier. In addition, the authors wish to acknowledge the advice of Dr. L. P. Goss concerning the reduction of two-colour PIV data. The authors wish to thank Dr. R. D. Hancock for assistance in assembly and construction of the burner. The authors also acknowledge Drs. R. D. Hancock, W. M. Roquemore, V. R. Katta, and K.-Y. Hsu for the stimulating discussions of vortex-flame dynamics. Finally, the authors wish to thank M. M. Whitaker for editing this manuscript. This work was supported by Air Force Contracts F33615-95-C-2507 and F33615-97-C-2702.

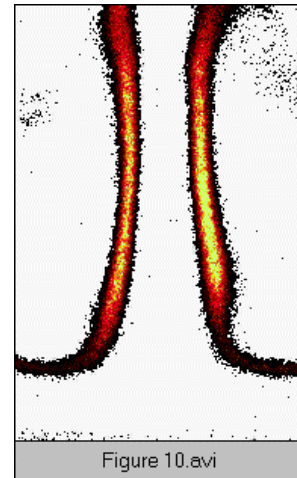


Figure 10: Animation corresponding to the frames of Figure 9.

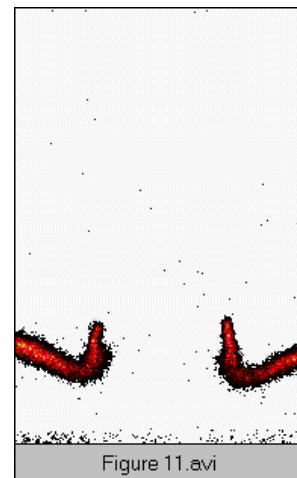


Figure 11: Animation using the same conditions as those for Figure 10, with an effective temporal spacing of  $10 \mu\text{s}$ . The temporal delay between the PLIF system and the

vortex corresponds to the region during which the Katta effect occurs.

## 7 References

- [1] Katta, V. R., Carter, C. D., Fiechtner, G. J., Roquemore, W. M., Gord, J. R., and Rolon, J. C., Interaction of a Vortex With a Flat Flame Formed Between Opposing Jets of Hydrogen and Air, accepted for publication in *Twenty-Seventh Symposium (International) on Combustion*, The Combustion Institute, Pittsburgh, 1998.
- [2] Hertzberg, J. R., Namazian, M., and Talbot, L., A Laser Tomographic Study of a Laminar Flame in a Karman Vortex Street, *Combustion Science and Technology*, Vol. 38, No. 3/4, pp. 205-216, 1984.
- [3] D. Escudie, Stability of a Premixed Laminar V-Shaped Flame, *Progress in Astronautics and Aeronautics*, Vol. 113, pp. 215-239, 1988.
- [4] Lee, T.-W., Lee, J. G., Nye, D. A., and Santavicca, D. A., Local Response and Surface Properties of Premixed Flames During Interactions with Karman Vortex Streets, *Combustion and Flame*, Vol. 94, No. 1/2, pp. 146-160, 1993.
- [5] Nye, D. A., Lee, J. G., Lee, T.-W., and Santavicca, D. A., Flame Stretch Measurements During the Interaction of Premixed Flames and Karman Vortex Streets Using PIV, *Combustion and Flame*, Vol. 94, No. 1/2, pp. 167-176, 1996.
- [6] Nguyen, Q.-V., and Paul, P. H., The Time Evolution of a Vortex-Flame Interaction Observed via Planar Imaging of CH and OH, *Twenty-Sixth Symposium (International) on Combustion*, The Combustion Institute, Pittsburgh, pp. 357-364, 1996.
- [7] Jarosinski, J., Lee, J. H. S., and Knystautas, R., Interaction of a Vortex Ring and a Laminar Flame, *Twenty-Second Symposium (International) on Combustion*, Pittsburgh, pp. 505-514, 1988.
- [8] Roberts, W. L., and Driscoll, J. F., A Laminar Vortex Interacting with a Premixed Flame: Measured Formation of Pockets of Reactants, *Combustion and Flame*, Vol. 87, No. 3/4, pp. 245-256, 1991.
- [9] Roberts, W. L., *A Premixed Laminar Flame Interacting With a Vortex Resulting in Flame Stretch and Quenching*, Ph.D. Dissertation, University of Michigan, Ann Arbor, 1992.
- [10] Roberts, W. L., Driscoll, J. F., Drake, M. C., and Ratcliffe, J. W., OH Fluorescence Images of the Quenching of a Premixed Flame During an Interaction with a Vortex, *Twenty-Fourth Symposium (International) on Combustion*, The Combustion Institute, Pittsburgh, pp. 169-176, 1992.
- [11] Driscoll, J. F., Sutkus, D. J., Roberts, W. L., Post, M. E., and Goss, L. P., The Strain Exerted by a Vortex on a Flame – Determined from Velocity Field Images, AIAA Paper No. 93-0362.
- [12] Roberts, W. L., Driscoll, J. F., Drake, M. C., and Goss, L. P., Images of the Quenching of a Flame by a Vortex – To Quantify Regimes of Turbulent Combustion, *Combustion and Flame* Vol. 94, No. 1/2, pp. 58-69, 1993.
- [13] Driscoll, J. F., Sutkus, D. J., Roberts, W. L., Post, M. E., and Goss, L. P., The Strain Exerted by a Vortex on a Flame – Determined from Velocity Field Images *Combustion Science and Technology* Vol. 4/6, pp. 213-229, 1994.
- [14] Mueller, C. J., Driscoll, J. F., Sutkus, D. J., Roberts, W. L., Drake, M. C., and Smooke, M. D., Effect of Unsteady Stretch Rate on OH Chemistry During a Vortex-Flame Interaction: To Assess Flamelet Models, *Combustion and Flame*, Vol. 100, No. 1/2, pp. 323-331, 1995.
- [15] Mueller, C. J., Driscoll, J. F., Ruess, D. L., and Drake, M. C., Effects of Unsteady Stretch on the Strength of a Freely-Propagating Flame Wrinkled by a Vortex, *Twenty-Sixth Symposium (International) on Combustion*, The Combustion Institute, Pittsburgh, pp. 347-355, 1996.
- [16] Mueller, C. J. *Measurements of Vortex-Flame Interaction Dynamics and Chemistry*, Ph.D. Dissertation, University of Michigan, Ann Arbor, 1996.
- [17] Sinibald, J. O., Mueller, C. J., Driscoll, J. F., Measured Local Propagation Velocities of Wrinkled Premixed Flames, proceedings of the *Fall Technical Meeting*, The Eastern States Section of the Combustion Institute, Hartford, CT, pp. 179-182, 1997.
- [18] Mueller, C. J., Driscoll, J. F., Ruess, D. L., Drake, M. C., and Rosalik, M. E., Vorticity Generation and Attenuation as Vortices Convect Through a Premixed Flame, *Combustion and Flame*, Vol. 112, No. 3, pp. 342-358, 1998.
- [19] Rolon, J. C., Aguerre, F., and Candel, S., Experiments on the Interaction Between a Vortex and a Strained Diffusion Flame, *Combustion and Flame*, Vol. 100, No. 3, pp. 422-429, 1995.
- [20] Thevenin, D., Rolon, J. C., Renard, P. H., Kendrick, D. W., Veynante, D., and Candel, S., Structure of a Non-Premixed Flame Interacting with Counterrotating Vortices, *Twentieth-Sixth Symposium (International) on Combustion*, The Combustion Institute, Pittsburgh, pp. 1079-1086, 1996.
- [21] Chen, S.-J., and Dahm, W. J. A., Vortex Ring/Diffusion Flame Interactions in Microgravity Conditions, proceedings of the *Fourth International Microgravity Combustion Workshop*, Cleveland, OH, pp. 191-196, 1997. NASA Conference Publication No. 10191.
- [22] See, for example: Najm, H. N., Paul, P. H., Mueller, C. J., and Wyckoff, P. S., On the Adequacy of Certain Experimental Observables as Measurements of Flame Burning Rate, *Combustion and Flame* Vol. 113, No. 3, pp. 312-332, 1998.

- [23] Gogineni, S., Goss, L., Pestian, D., and Rivir, R., Two-Color Digital PIV Employing a Single CCD Camera, *Experiments in Fluids*, in press, 1998.
- [24] Donbar, J. M., *Reaction Zone Structure and Velocity Measurements in Permanently Blue Nonpremixed Jet Flames*, Ph.D. Dissertation, University of Michigan, Ann Arbor, 1998.
- [25] R. P. Khosla, From Photons to Bits, *Physics Today*, Vol. 45, No. 12, pp. 42-49, 1992.